Renewable Energy 80 (2015) 690–698

Contents lists available at ScienceDirect

Renewable Energy

journal homepage: www.elsevier.com/locate/renene

Investigation of the performance of a staggered configuration of tidal turbines using CFD

Mulualem G. Gebreslassie*, Gavin R. Tabor, Michael R. Belmont

College of Engineering, Mathematics and Physical Sciences, University of Exeter, North Park Road, Exeter EX4 4QF, United Kingdom

ARTICLE INFO

Article history:
Received 5 June 2014
Accepted 1 March 2015
Available online 18 March 2015

Keywords:
CFD
IBF model
Power extraction
Wake interaction
Blockage

ABSTRACT

This paper investigates the influence of wake interaction and blockage on the performance of individual turbines in a staggered configuration in a tidal stream farm using the CFD based Immersed Body Force turbine modelling method. The inflow condition to each turbine is unknown in advance making it difficult to apply the correct loading to individual devices. In such cases, it is necessary to establish an appropriate range of operating points by varying the loading or body forces in order to understand the influence of wake interaction and blockage on the performance of the individual devices. The performance of the downstream turbines was heavily affected by the wake interaction from the upstream turbines, though there were accelerated regions within the farm which could be potentially used to increase the overall power extraction from the farm. Laterally closely packed turbines can improve the performance of those turbines due to the blockage effect, but this could also affect the performance of downstream turbines. Thus balancing both the effect of blockage and wake interaction continues to be a huge challenge for optimising the performance of devices in a tidal stream farm.

1. Introduction

The study of turbine to turbine interaction is crucial to understand how energy shadowing of an array of devices influences energy extraction by the individual devices. Simple turbine to turbine interactions can be investigated using small scale experiments on two or three turbines, but the feasibility of experimental studies with multiple devices in a tidal stream farm is challenging due to the practical and cost implications of an experiment involving tens of devices within a sufficiently large flow domain. Consequently, researchers are focusing on exploring alternative methods to investigate the flow features around tidal turbines. Computational Fluid Dynamics (CFD) studies currently represent an interesting alternative for these kind of studies.

The study of wake interactions of wind turbines using both analytical and CFD techniques is well documented as this technology has been in the forefront for many years [1–6]. Recently there have been several efforts to apply similar techniques to investigate the wake interactions of turbines in tidal stream farms, taking into account the fundamental differences in the working environments between the two technologies. As in the experimental approach, there are computational cost aspects which come into play when CFD techniques are used to study the flow features of groups of turbines. For single turbine simulations either in wind or tidal turbines, it is possible to employ detailed modelling techniques such as tracking the individual blade motions with current computational resources. As the number of devices increases, such as in the study of arrays of devices, the computational cost spirals and detailed blade modelling becomes impractical. In such cases we must investigate lower cost turbine modelling such as actuator disk methods.

Study by Ref. [7] used a blade element and actuator disc method to investigate the wake interaction of a tidal stream farm with 5 rows of turbines configured in the stream-wise direction. This study showed that the power coefficient of the second row was lower than the rest of the devices due to huge wake interaction from the first row, but the turbines from the third row onwards showed better power coefficients due to high wake recovery within the array. Those comparisons have been made based on a single resistance coefficient. Study of a staggered configuration of arrays of devices by Refs. [8,9] showed an acceleration of the bypass flows due to the venturi created by the turbines which is important to improve the performance of any downstream devices. A similar study by Ref. [10] observed that a staggered configurations of

* Corresponding author.
E-mail address: mgg204@ex.ac.uk (M.G. Gebreslassie).

http://dx.doi.org/10.1016/j.renene.2015.03.001

turbines with a small longitudinal spacing offers high efficiency. Experimental studies of arrays of devices by Refs. [11,12] also showed that with a particular inter-turbine spacing there is the potential of accelerated flow regions which can be used for high power production by deploying turbines in those regions [12]. particularly indicated a flow acceleration of up to 14% can be achieved due to the presence of arrays of devices. The experimental work also reveals there is less wake propagation downstream of single row of turbines if the lateral spacing is increased, otherwise laterally closely spaced turbines would produce a huge plug flow of slow water which could affect the performance of downstream devices. They have suggested that an off-set or staggered configuration would provide a better option and allow longitudinally closely packed devices to be deployed with less wake interaction and possibly higher power extraction due to accelerated bypass flows. These studies indicated the importance of analysing the influence of turbine to turbine interactions of arrays of devices in order to optimize the power extraction.

Calibration of the energy extraction in a tidal stream farm inevitably depends upon the inflow conditions to each devices. Given that the turbines interact with each other these inlet conditions are themselves unknown at the start of the calculation, which makes it difficult to apply the correct resistance coefficient to each of the downstream row of turbines. The aim of this study is therefore to obtain a range of operating points for turbines in a staggered configuration tidal stream farm. The turbine analysed is the cross flow Momentum-Reversal-Lift tidal turbine [13], a novel design intended for use in shallow estuaries in large farm installations (100 + turbines). Relative comparisons of the power extraction by a base case tidal turbine and turbines in a tidal farm was also carried out to understand the influence of wake interactions on the performance of individual devices.

2. Methodology

Several comparisons of LES and RANS modelling techniques have been reported due to their increased importance in modelling turbulent flows. It is generally agreed that RANS is the simpler technique but it lacks accuracy especially in applications where there are more complex flows such as vortex shedding, large separation zones, and high streamline curvature [14–17]. In particular, RANS relies on an implicit assumption that there is a scale separation between all turbulent components of the flow, which will be replaced by a statistical model, and any deterministic transient motions such as vortex shedding, pulsatile pumping or (as here) flow components associated with the blade motions. In cases such as this one where there is a significant overlap between the deterministic and large turbulent scales, LES is known to be the preferred approach. Despite this, an initial set of simulations was conducted for the new MRL device in order to compare the two modelling techniques for this turbine. The analysis indicated that the LES modelling technique showed better results for the MRL device. The detailed discussions and comparisons of the two models are reported in Ref. [13]. Thus the LES modelling technique has been implemented for this research work.

2.1. Large eddy simulation

The Large Eddy Simulation (LES) modelling approach resolves the large-scale turbulent motions by filtering the Navier-Stokes equations, and the small-scale motions are modelled using Sub-Grid Scale (SGS) models [18–20]. It is generally accepted that the small scale motions in turbulent flow, whilst most numerous, are similar from place to place in the flow and across different flow types, and thus can accurately be replaced by a statistical model. The resolved (Grid Scale) motions, either deterministic or turbulent, are case specific and thus have to be explicitly resolved [21]. The body force (F_b, see details in 2.2) applied by a turbine against the flow is implemented as source term in the LES equation of momentum conservation (1), and solved together with a mass continuity Equation (2). The source terms are only applied in cells within the turbine blade regions. The LES governing equations are a combination of filtered Navier-Stokes equations and the source terms written as:

$$\frac{\partial \overline{u}_i}{\partial t} + \frac{\partial}{\partial x_j}\left(\overline{u}_i \overline{u}_j\right) = -\frac{1}{\rho}\left(\frac{\partial \overline{p}}{\partial x_i} + \delta_{i1}\frac{\partial \langle P \rangle}{\partial x_1}\right) + 2\nu \frac{\partial}{\partial x_j}\overline{S}_{ij} - \frac{\partial \tau_{ij}}{\partial x_j} + \rho g_i + \overline{F}_s + \overline{F}_b \tag{1}$$

The continuity equation is given as:

$$\frac{\partial \overline{u}_i}{\partial x_i} = 0 \tag{2}$$

Where the bar $\overline{(\cdot)}$ defines the resolved scales; $\overline{u}$ is the filtered velocity, $\overline{p}$ is the filtered pressure; ν is a kinematic viscosity; δ_{i1} is the Kronecker-delta and $\frac{\partial \langle P \rangle}{\partial x_1}$ is the driving force, a constant streamwise pressure gradient, τ_{ij} is the SGS Reynolds stress. $\overline{S}_{ij}$ is the strain rate of the large scales or resolved scales and is defined as:

$$\overline{S}_{ij} = \frac{1}{2}\left(\frac{\partial \overline{u}_i}{\partial x_j} + \frac{\partial \overline{u}_i}{\partial x_i}\right) \tag{3}$$

The resulting SGS stresses from the filtering processes are unknown and need modelling. These stresses represent large scale momentum fluxes resulting from the unresolved scales. Most of the time, these stresses have been approximated by SGS models based on the eddy viscosity concept. The most commonly employed hypothesis in the SGS turbulence models is the Boussinesq hypothesis [22] which calculates the SGS stress as a linear function of the rate of strain tensor. Popular SGS models include the Smagorinsky model, the one equation eddy viscosity, and dynamic variants of these, in which the model coefficients can be evaluated mathematically using grid scale information. A study by Ref. [23] showed that the one-equation eddy viscosity model is much better than the Smagorinsky model because of its weak dependence on the filter width and Reynolds number and therefore is suited for applications in coarse grid LES. Thus, this SGS model was implemented in this study.

The one-equation eddy viscosity model developed by Ref. [24] has been used in a wide range of turbulent problems. Based on [24], the Sub-Grid stresses are defined as:

$$\tau_{ij} = \frac{2}{3}k_{sgs}\delta_{ij} - 2\nu_t \overline{S}_{ij} \tag{4}$$

where ν_t is the SGS eddy viscosity given as:

$$\nu_t = C_k \overline{\Delta}\sqrt{k_{sgs}} \tag{5}$$

and the SGS kinetic energy, k_{sgs}, is given as:

$$k_{sgs} = \frac{1}{2}\left(\overline{u_i u_i} - \overline{u}_i \overline{u}_i\right) \tag{6}$$

The transport equation for the SGS kinetic energy is defined as [23]:

$$\frac{\partial k_{sgs}}{\partial t} + \overline{u}_i \frac{\partial k_{sgs}}{\partial x_i} = -\tau_{ij}\frac{\partial \overline{u}_i}{\partial x_j} - C_c \frac{k_{sgs}^{3/2}}{\overline{\Delta}} + \frac{\partial}{\partial x_i}\left(\frac{\nu_t}{\sigma_k}\frac{\partial k_{sgs}}{\partial x_i}\right) \tag{7}$$

where $C_k = 0.05$, $C_c = 1.0$, and $\sigma_k = 1.0$ based on [23]. However, different values of the model coefficient C_k have been used in other studies such as $C_k = 0.094$ by Ref. [25], C_k=0.1 by Ref. [26]. However, sensitivity analysis carried out with different value of C_k showed no huge difference on the results and thus $C_k = 0.094$ was used for all the simulations in this study.

The MRL turbine is designed to operate relatively close to the water surface and therefore the dynamics of the free surface is important to understand the overall behaviour of the turbine. The Volume of Fluid (VOF) method is a model used to determine the dynamics of free surface flow problems and has been widely used in the study of floating body applications, breaking waves, non linear free surface flows and other multiphase flows as documented by Refs. [27–30]. In the VOF method, a single set of flow equations is solved for a mixture fluid, together with an indicator function γ representing the degree to which one of the phases is present in each cell (ranging from γ=1 representing the complete presence of one phase in the cell, to γ=0 representing its complete absence). The location of the interface can then be deduced from the γ field. This method, which is an easy, flexible and efficient method for treating free boundaries [31], was used to account for the impact of the free surface on the turbine.

2.2. Turbine modelling

Most researchers accept that simple momentum sink zone models such as actuator disc methods are crude and make it difficult to incorporate energy loss processes. However, because of their lower computational cost they are the few computationally realistic approaches for gaining insight into the behaviour of substantial clusters of devices. This study builds upon this accepted methodology by incorporating additional modelling features that induce energy absorption from the flow, providing a downstream wake structure which reflects more closely that of the real turbines. The model adopted is referred to as the Immersed Body Force (IBF) model, which is a novel turbine modelling technique developed by the authors of this paper. It has been already utilised for modelling individual turbines and small groups of turbines as shown in Refs. [32–34]. For the IBF approach, a body force function per unit volume of the blades (F_b) representing the resistance by the turbine against the flow is introduced to create momentum change. The detailed modelling was developed by considering drag (F_{RD}) and lift (F_{RD}) resistance forces applied by the blades against the fluid flow as:

$$\overline{F}_b = \overline{F}_{RD} + \overline{F}_{RL} \tag{8}$$

Detailed information about this model can be found in Ref. [13]. This empirically-based model has been calibrated against experiment and found to perform well, although we recognise that it does not necessarily fully reproduce all the large scale deterministic flow patterns in the way that a dynamic blade motion simulation would do. However such a blade motion simulation would be orders of magnitude more expensive to calculate, and the IBF is thus computationally cheap enough to allow multiple turbine simulations to be run.

Avoiding modelling the blade motions means that pressure integration over the blade surface can not be used to directly estimate the mechanical power absorbed by the machine from the flow. Consequently, published research on simplified descriptions of turbines of all kinds has focussed upon calculating the energy lost from the flow. Typical examples of this are the various developments of momentum sink models (e.g. actuator disc descriptions) or Darcy flow based models that implicitly represent the turbine by a viscous dissipation sink region. Examples of this approach are given in Refs. [35–38]. A similar approach has been undertaken in the work presented here, as will be discussed below.

Calibration of the energy extraction by the turbine inevitably depends upon the inflow conditions. Given that the turbines interact with each other these inlet conditions are themselves unknown at the start of the calculation which makes it difficult to apply the correct body force to each of the downstream row of turbines. For this reason, the best option is to apply different body forces to obtain the power curve for each turbine in the farm in order to understand their range of operating points. The body force is applied in the axial and vertical direction giving a complex energy removal. For this kind of complex energy removal, the total thrust force experienced by the turbine can be properly evaluated by calculating the change in flux across the turbine region by applying Conservation of Linear Momentum (COLM) over a control volume. The turbine is enclosed in a rectangular control volume shown in Fig. 1 in order to calculate the momentum flux on each face of the control volume.

Recent studies showed that turbines in a constrained flow have better performance compared to those in unconstrained flow due to an additional power contribution by the static pressure gradient in the streamwise direction as documented in Refs. [39–42]. Thus the power available to the device includes a contribution from the static pressure and dynamic heads. Applying COLM over the rectangular control volume, the thrust force acting on the device can be defined as:

$$T = \int_{A_{yz}} \left[(p)|_x - (p)|_{x+\Delta x}\right] dA + \int_{A_{yz}} \left[(\rho u_x u_x)|_x - (\rho u_x u_x)|_{x+\Delta x}\right] dA + \int_{A_{xz}} \left[(\rho u_y u_x)\big|_y - (\rho u_y u_x)\big|_{y+\Delta y}\right] dA + \int_{A_{xy}} \left[(\rho u_z u_x)|_z - (\rho u_z u_x)|_{z+\Delta z}\right] dA \tag{9}$$

where T is the thrust force on the turbine. The velocity of the flow at the $-$ith boundary face located at point x is given by $u_x|_x$. The mass flux entering into the face of the $-$ith boundary is only due to the velocity component normal to the face (i.e., u_x) which is given by $(\rho u_x)|_x$. This results a linear momentum flux of $(\rho u_x u_x)|_x$ at the $-\mathbf{i}$ boundary. The linear momentum flux for the rest of the boundary faces can be evaluated in a similar manner. Based on this, the thrust force on the turbine can be evaluated using an appropriate control volume enclosing the turbine.

The power removed by the turbine from the flow is defined using the thrust force as:

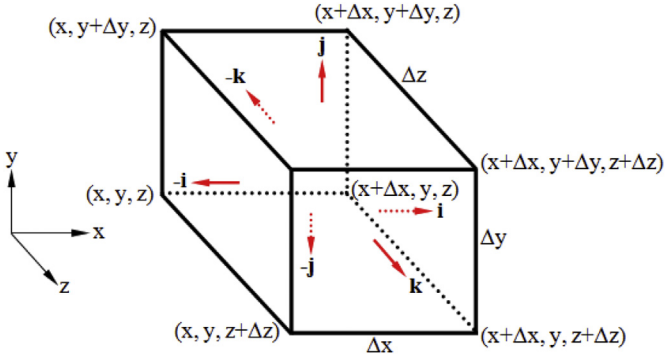

Fig. 1. Demonstration of the 3-D representation of a control volume housing the turbine.

$$P = T\overline{u_t} \tag{10}$$

Note that this power removed from the flow is a combination of the useful power that is used to drive the generator and the power loss within the turbine region. In the actuator disc method, the average velocity, $\overline{u_t}$, is commonly calculated by averaging the velocity over the area of the disc because of the uniform characteristics of the resistance coefficient. However, the density of the body forces in the IBF model are not uniform on the turbine region, and thus the velocity is averaged over the volume occupied by the turbine as:

$$\overline{u_t} = \frac{1}{V}\int_V u_x dV \tag{11}$$

where V is the total volume of the turbine region. This method of calculating the average velocity value gives better representation of the velocity within the turbine housing. The axial induction factor (a) is a measure of the reduction of the velocity at the turbine compared to that of the upstream velocity which is calculated as:

$$a = \frac{u_\infty - u_t}{u_\infty} \tag{12}$$

where u_∞ is the far upstream velocity and u_t is the velocity at the turbine.

3. Model set-up

The Momentum-Reversal-Lift turbine (Fig. 2) has an overall diameter of D = 0.20 m and a length of L = 0.30 m. The blades have maximum thickness and chord length of 1.7 cm and 9.5 cm respectively. The domain overall height is 8.3125D. The spacing between the turbine and the wall boundary on both sides is 5D. The spacing between the turbine with the bottom wall boundary and the free surface are 4.175D and 1D respectively. Solution of the LES and VOF model equations was performed using the open source Finite Volume code OpenFOAM [43]. Two models were constructed; a base case simulation consisting of a single turbine in the channel and a group of 7 turbines laid out as shown in Fig. 3. The turbines are labelled to identify their positions for the subsequent discussions as T1, T2 etc.

The power extraction for the single turbine simulation was monitored to evaluate convergence and mesh dependency of the solutions using different mesh densities. Assuming that the highest mesh resolution provides the most accurate indicator of the performance of the turbine, the power was observed to vary between 0.17% and 1.15%. With the computational cost being as a factor, a mesh size of 156,848 elements, which has an error of 0.17%, was selected for the base case single turbine simulations. Based on this observation, the seven turbine farm simulation was developed with 1,013,264 cells and fine mesh resolution was used around the zone of interest. The initial condition of the whole domain is considered to consist of two fluid phases, water and air with the water level being at 6.3125D from the bottom of the domain and the rest of the domain is occupied by air.

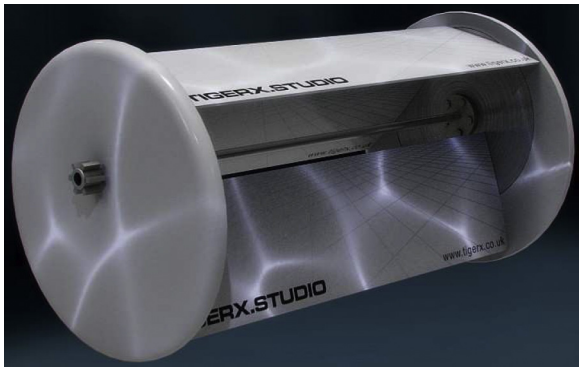

Fig. 2. A prototype of Momentum-Reversal-Lift type of horizontal axis tidal turbine.

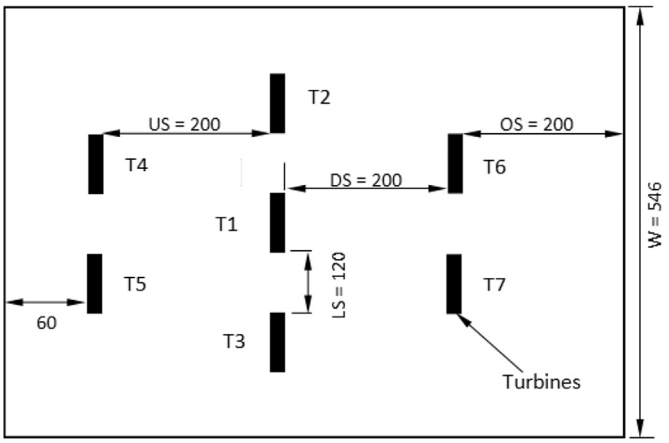

Fig. 3. Seven turbine configuration with the units of the dimensions in millimetre.

A list of the longitudinal and lateral spacings for the turbines in the array are given in Table 1. The Upstream Spacing (US) represents the longitudinal spacing between the upstream and middle turbines, Downstream Spacing (DS) represents the longitudinal spacing between the middle and downstream turbines, Outlet Spacing (OS) represents the longitudinal spacing between the downstream turbines and the outlet of the domain, Lateral Spacing (LS) represents the lateral spacing between turbines, and W represents width of the domain as shown in Fig. 3 with the units of the dimensions being in millimetre (mm).

The blockage ratio given in the table is calculated considering the combined cross-sectional area of the individual turbines which block different stream-tube flows and the cross-sectional area of the channel. Based on this calculation the blockage ratio for the single and seven turbine configurations are B=0.021 and B=0.044 respectively.

The IBF model was validated with experimental results and with different turbine modelling technique known as GGI conducted to establish the performance of the MRL turbine as shown in Ref. [13]. Although the experiments and the numerical calculation were conducted in relatively higher blockage ratio compared to the one used in this study, there is high confidence on the numerical model to be valid for any other computational dimensions. Thus the results from the single turbine simulation has been used as a base case to investigate and compare the influence of wake interactions on the performance of individual turbines in the tidal stream farm, which is typical and common way of getting some insight about the behaviour of tidal farms because of the high cost implications of experimental works.

Table 1
Longitudinal and lateral spacing of the computational domain.

Configuration	Spacing					Blockage ratio (B)
	US	DS	OS	LS	W	
Base case	0D	0D	20D	0D	11.5D	0.021
Seven turbines	10D	10D	10D	6D	27.3D	0.044

The computational domain contains seven boundary patches, namely atmosphere, seabed, wall, waterInlet, airInlet, and outlet. The top part of the domain was air, bounded above by a boundary condition allowing both outflow and inflow according to the internal flow. seaBed and wall are the floor and the front and back side of the computational domain respectively and both patches represent wall boundary conditions. The waterInlet and airInlet are the patches where the water and air enter to the computational domain respectively. The outlet is the patch where both fluids flow out of the computational domain.

The turbine performance depends on the vertical velocity distribution as the inflow velocity is not uniform across the depth of the water column. This inflow velocity is represented by power law velocity profile as it gives good approximations for most tidal current sites. As this study is not focused on specific site, it is appropriate to implement this general power law, which is discussed in detail in Ref. [13]. Thus the power extraction have been calculated based on the vertical velocity distribution represented by the power law along the swept area of the device.

4. Results and discussions

4.1. Flow field analysis

Plan views of the velocity contours of a base case turbine simulation at different body forces are shown in Fig. 4. To analyse the flow field and performance of the turbine a range of forces were imposed in order to predict the power curve or power characteristics of the turbine. None or Maximum force can be imposed until a point where the power extraction by the turbine becomes zero. However, it wasn't necessary to do calculations for zero power extraction because of the computational cost. For this reason the cubic relationship between the power and the stream velocity was obtained by varying the forces with the peak power being in between two extreme loadings (minimum and maximum forces). Thus all the body forces were normalised by the maximum body force (Normalised body force (NBF) = F_b/F_{bmax}). At higher body forces, there is a huge velocity deficit immediately downstream of the turbine but the wake recovers faster than is the case for lower body forces. This has a profound effect on building tidal stream farms with the correct body forces that give the optimal power extraction, as the inflow conditions to individual devices is unknown in advance because of the wake interactions. One way of finding the correct body forces is to find a range of operating points for the individual devices in the farm by varying the body forces. During this process, a full picture of the flow characteristics of the farm guides where the optimal operating points would be for individual turbines.

Results from the single turbine simulations were used for guidance because of the lack of experimental data to understand the relative effect of turbines in a tidal stream farm. Fig. 5 shows plan views of the velocity contours of staggered configurations of seven turbines for different body forces. The flow characteristics for different body forces showed similar trends to the results for the base case turbine. However, the effect of wake interaction on the flow conditions of individual devices is now visible in those seven turbine cases. At higher body forces, there is a faster wake recovery, which minimises the effect of wake interactions on downstream devices leading to a similar velocity deficit immediately downstream of each turbine. In contrast, at lower body forces there is a slower wake recovery resulting a huge influence of the wake interaction on the downstream turbines (T6 and T7). The difference is clearly shown in Fig. 5c–e, where there is a huge velocity deficit immediately downstream of T6 and T7.

Detailed velocity data was extracted both in the stream-wise and span-wise directions through the center of the turbines to understand the effect of the blockage and wake interaction on the flow conditions of the farm. Fig. 6 shows the velocity profiles through the centreline of the upstream turbines (T4 and T5), middle turbines (T1, T2, and T3) and downstream turbines (T6 and

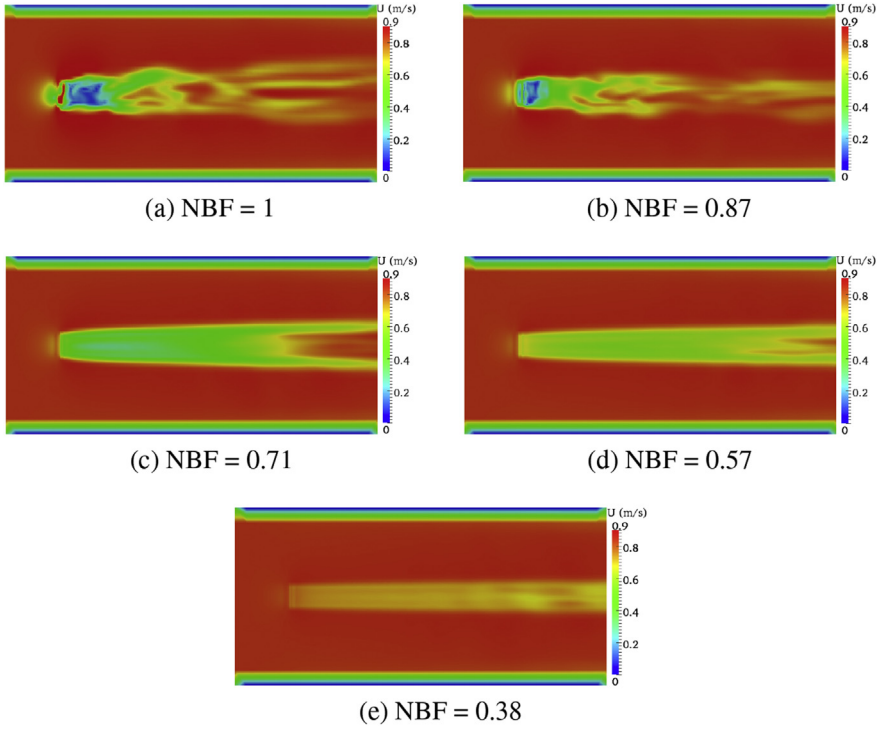

Fig. 4. Snapshots of velocity contours of a single turbine at different loadings.

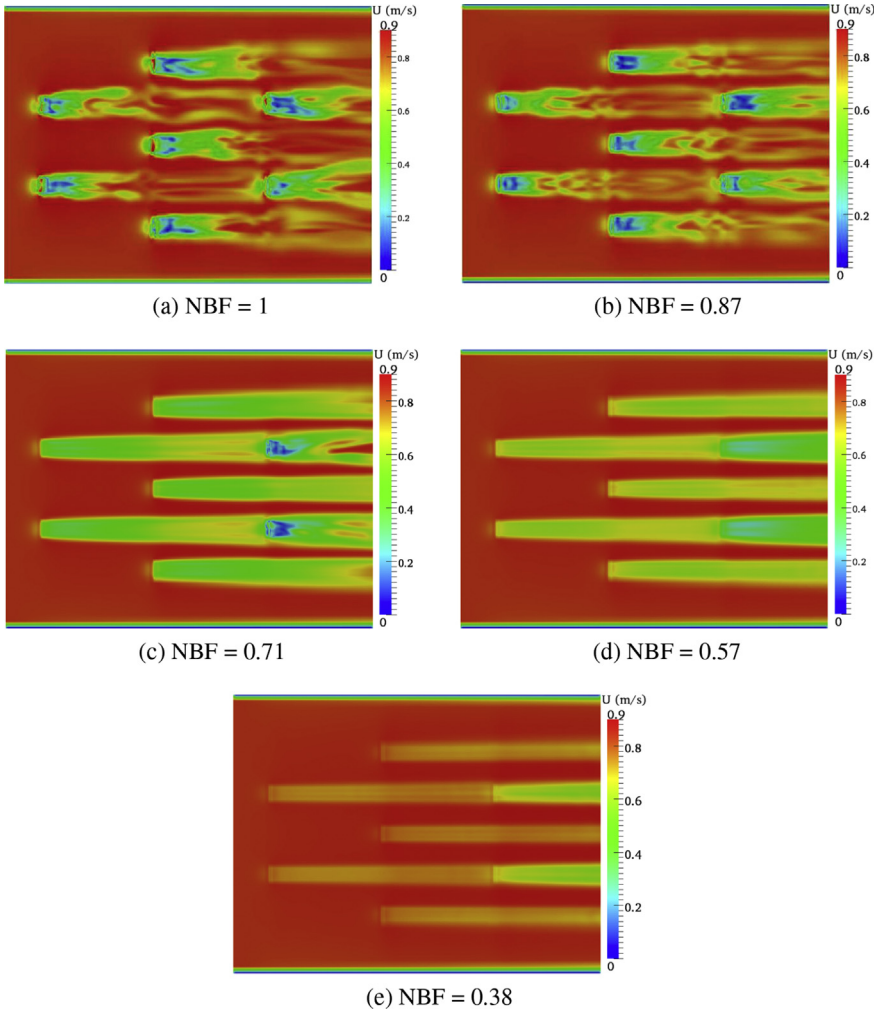

Fig. 5. Snapshots of velocity contours of seven turbines at different loadings.

T7) along the span-wise direction. It is obvious from the graph that the velocity deficit at the center of the turbines is higher at higher body forces (NBF = 1) compared to the same turbines at lower body forces. However, at higher body forces the bypass flow between turbines 4 and 5 is higher than at lower body forces leading to lower velocity deficit at the center of T1. This has direct effect on the performance of that turbine. The other observation from this graph is that at lower body forces (NBF = 0.38) the bypass flow between T6 and T7 is lower than at higher body forces which is directly related to the slower wake recovery from T1.

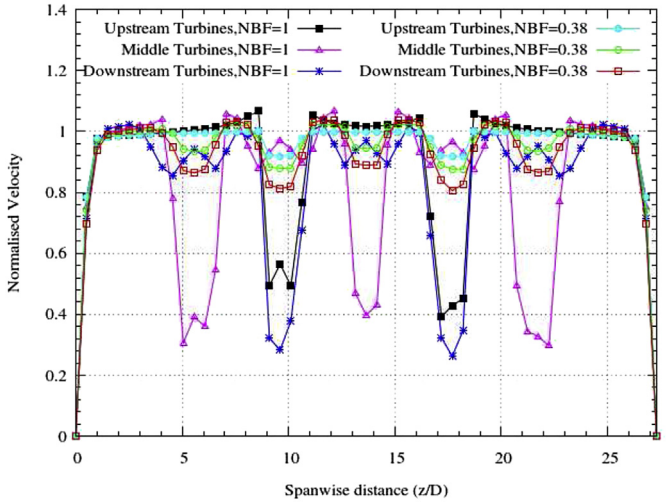

Fig. 6. Span-wise flow profiles through the centreline of the turbines in the farm at NBF = 1 and NBF = 0.38.

Stream-wise velocity profiles through the center of T1 at different body forces also showed a similar trend as shown in Fig. 7. At higher body forces, the wake recovers faster but also creates accelerated bypass regions as shown between the regions from 2D–11D.

Comparison of velocity profiles through each turbine in the farm and the base case turbine at NBF = 1 is given in Fig. 8. The graph clearly shows that the incident velocities to the middle turbines (around 11D) is higher than the incident velocity to the base case turbine which is due to the accelerating bypass flow created by the upstream turbines. The incident velocity of the base case turbine is higher than the incident velocity to the downstream turbines as shown around 22D because of the wake interaction from the upstream turbines. However, the incident velocities to the base case and upstream turbines is similar as expected.

4.2. Thrust and power analysis

Influence of the blockage and wake interaction on the performance of individual turbines in the farm was analysed in detail

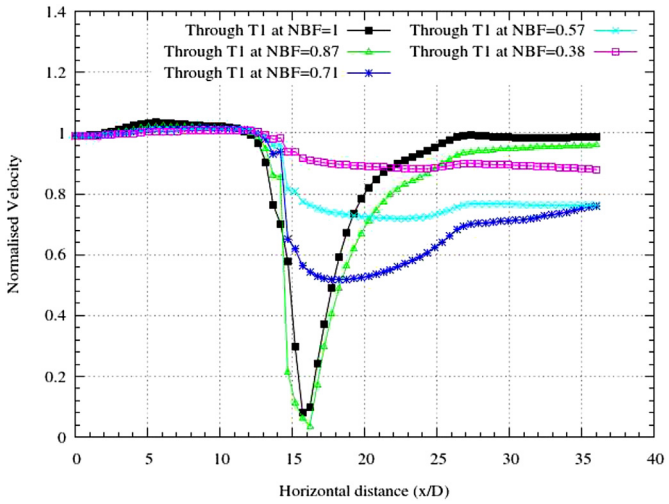

Fig. 7. Stream-wise flow profiles through the centreline of turbine 1 at different body forces.

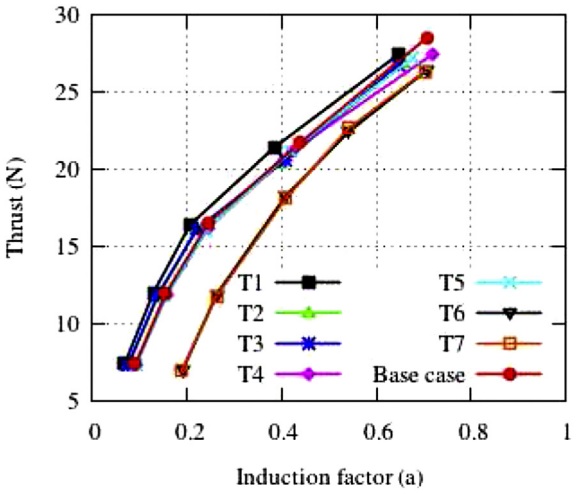

Fig. 9. Comparison of thrust forces experienced by the turbines in the base case and the farm.

using the thrust experienced by the turbines and their corresponding power extraction. Fig. 9 shows a comparison of the thrust forces experienced by the turbines both in the base case and farm configurations, against induction factor. The thrust force experienced by T1 in the farm is higher than the thrust force experienced by the other turbines leading to higher power extraction, while T6 and T7 experienced lower thrust force compared to the others. This trend is also reflected in the power characteristics of each turbine as shown in Fig. 10.

Power curves for all the turbines are shown in Fig. 10 against an axial induction factor. The results showed a wide range of differences in power extraction between the individual turbines. The power extraction by the upstream turbines (T4 and T5) is slightly lower than the power from the base case turbine. Although there is no wake interaction effect to those turbines there is a strong possibility that there has been an effect on their performance due to the presence of the downstream turbines, no matter what the configuration of those turbines is. The blockage effect of those laterally spaced turbines could have improved their performance as the blockage has a positive impact on the performance of individual devices packed laterally. However, closely spaced downstream devices can have a negative impact on the performance of upstream turbines due to their blockage effect which is the main reason for the lower power extraction by the upstream turbines compared to the base case turbine, though the difference is very small.

Power extraction by the third row of turbines (T6 and T7) is much lower than the power extraction by the rest of the turbines which is mainly affected by the wake interaction from the upstream turbines. However, as the induction factor increases, meaning with an increased body force, the difference of the power extraction decreases. As previously mentioned in the flow analysis, the wake recovers faster at higher body forces thus minimising the wake interaction with downstream devices which reduces the power extraction difference seen at higher induction factors. The peak power extraction by the downstream turbines also occurs at higher induction factor compared to the other turbines.

Performance of T1 in the farm is higher than the rest of the turbines for every operating point. There are two potential reasons for the high performance of T1. Firstly, it is located downstream of the bypass flow region between T4 and T6 and the accelerating flow created within this bypass flow region can significantly improve its

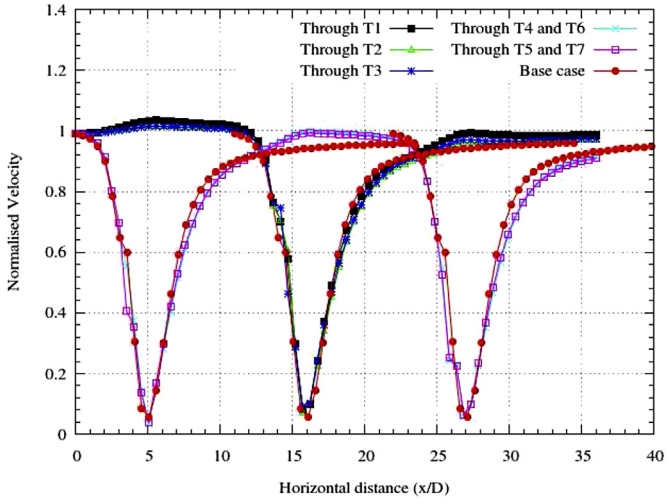

Fig. 8. Stream-wise flow profiles through the centreline of the turbines in the base case and the farm at NBF = 1.

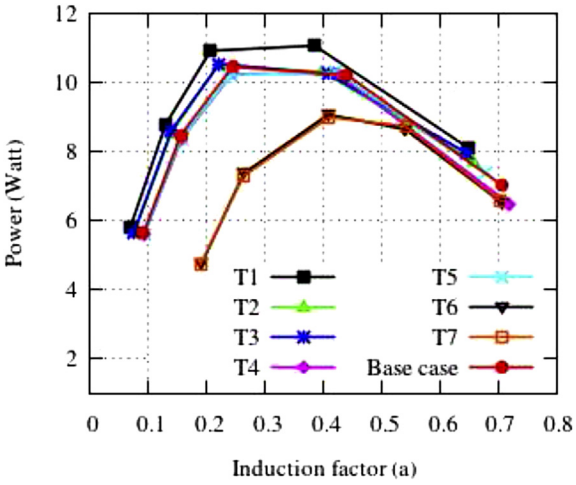

Fig. 10. Comparison of power extraction by the turbines in the base case and the farm.

performance. This is one of the big advantages to maximize the overall power extraction from a tidal stream farm by positioning turbines in the accelerating regions. Secondly, the power extraction of turbines can be improved by having a high blockage ratio and the fact that there are three turbines laterally sited in this region means that the performance of T1 could be also improved due to the blockage ratio. T2 and T3, which are part of the middle row of turbines, have also shown higher power extraction compared to the base case turbine for a similar reason where the accelerating flow is now on the other side of T4 and T5. High blockage ratio does not necessary mean that the overall power extraction from a tidal stream farm can be higher because when the blockage ratio is increased, there is a risk of losing accelerating flow regions and a high possibility of wake interaction on downstream devices. This normally requires longer stream-wise spacing between the turbines to avoid the wake interaction, which is contra-indicated especially in places where there are spatial constraints for deployment of the turbines.

This detailed analysis in general shows that the peak power from the individual turbines in the farm occurs at different operating points, meaning at different body forces. However, doing a detailed analysis at different body forces for hundreds of devices is unrealistic due to the high computational cost. The other problem is that as the inflow conditions are unknown in advance it is also difficult to apply the correct body force to give the possible maximum power extraction from each turbine. One of the potential options is therefore to design a computationally feasible representation of small arrays of turbines and do a similar analysis to explore the behaviour of the turbines and obtain their maximum operating points. These data can be then used as a base for optimisation tools to maximise the power extraction from hundreds of devices in a tidal stream farm.

5. Conclusion

A model of a small (7 turbine) tidal stream farm was constructed to investigate the influence of wake interaction on the performance of individual devices. The results were compared with a base case simulation to understand the relative influence of additional turbines in a tidal stream farm. This study has provided valuable information on how to identify the maximum operating points of turbines in cases where the inlet flow conditions to each turbine is unknown in advance. It is necessary to establish an appropriate range of operating points by varying the body forces in order to understand the influence of wake interaction and blockage. The performance of downstream turbines was heavily affected by the wake interaction from the upstream turbines, though there were accelerated regions within the farm which could be potentially used to increase the overall power extraction from the farm. With restricted sites available for deployment of tidal turbines, the wake interaction could be a major problem and using a staggered configuration might help along with closely packed turbines in the stream-wise direction, provided that if there is appropriate bypass flow regions where the turbines located in those regions can gain an advantage from the accelerating flows. High performance can be achieved by using laterally closely packed configuration turbines, but such kind of configuration can affect the performance of downstream turbines. This makes balancing the effect of both blockage and wake interaction one of the challenging issues in optimising the location of devices in a tidal stream farm.

Acknowledgement

This study is funded by EPSRC, project number EP/J010138/1, under the Supergen Marine research program.

References

[1] Méchali Martin, Barthelmie Rebecca, Frandsen Sten, Réthoré PE. Wake effects at horns rev and their influence on energy production. In: European wind energy conference and exhibition; 2006. p. 10.
[2] Barthelmie RJ, Larsen GC, Frandsen ST, Folkerts L, Rados K, Pryor SC, et al. Comparison of wake model simulations with offshore wind turbine wake profiles measured by sodar. J Atmos Ocean Technol 2006;23(7):888–901.
[3] Barthelmie Rebecca Jane, Hansen K, Frandsen Sten Tronæs, Rathmann Ole, Schepers JG, Schlez W, et al. Modelling and measuring flow and wind turbine wakes in large wind farms offshore. Wind Energy 2009;12(5):431–44.
[4] Rathmann Ole, Frandsen Sten Tronæs, Barthelmie Rebecca Jane. Wake modelling for intermediate and large wind farms. 2007.
[5] Ainslie John F. Calculating the flowfield in the wake of wind turbines. J Wind Eng Industrial Aerodynamics 1988;27(1):213–24.
[6] Troldborg Niels, Larsen Gunner C, Madsen Helge A, Hansen Kurt S, Sørensen Jens N, Mikkelsen Robert. Numerical simulations of wake interaction between two wind turbines at various inflow conditions. Wind Energy 2011;14(7):859–76.
[7] Harrison ME, Batten WMJ, Bahaj AS. A blade element actuator disc approach applied to tidal stream turbines. In: OCEANS 2010. IEEE; 2010. p. 1–8.
[8] Bai L, Spence RRG, Dudziak G. Investigation of the influence of array arrangement and spacing on tidal energy converter (TEC) performance using a 3-dimensional CFD model. In: Proceedings of the 8th European wave and tidal energy conference, Uppsala, Sweden; 2009.
[9] Batten WMJ, Bahaj AS. Cfd simulation of a small farm of horizontal axis marine current turbines. In: Proceedings world renewable energy congress WREC IX. Elsevier Science; 2006.
[10] Churchfield MJ, Li Y, Moriarty PJ. A large-eddy simulation study of wake propagation and power production in an array of tidal-current turbines. 2011.
[11] Myers LE, Keogh B, Bahaj AS. Experimental investigation of inter-array wake properties in early tidal turbine arrays. In: OCEANS 2011. IEEE; 2011. p. 1–8.
[12] Daly T, Myers LE, Bahaj ABS. Experimental investigation of the effects of the presence and operation of tidal turbine arrays in a split tidal channel. Mar Ocean Technol 2011;9:2262.
[13] Gebreslassie Mulualem Gebregiorgis. Simplified CFD modelling of tidal turbines for exploring arrays of devices [PhD thesis]. University of Exeter; 2012.
[14] Wilcox David C. Turbulence modelin for CFD. DCW Industries, Inc; 1998.
[15] Cheng Y, Lien FS, Yee E, Sinclair R. A comparison of large eddy simulations with a standard k–ε reynolds-averaged navier–stokes model for the prediction of a fully developed turbulent flow over a matrix of cubes. J Wind Eng Industrial Aerodynamics 2003;91(11):1301–28.
[16] Mihaescu M, Murugappan S, Kalra M, Khosla S, Gutmark E. Large eddy simulation and reynolds-averaged navier–stokes modeling of flow in a realistic pharyngeal airway model: an investigation of obstructive sleep apnea. J biomechanics 2008;41(10):2279–88.
[17] Breuer M, Jovičić N, Mazaev K. Comparison of DES, RANS and LES for the separated flow around a flat plate at high incidence. Int J Numer methods fluids 2003;41(4):357–88.
[18] Moin P, Kim J. Numerical investigation of turbulent channel flow. J Fluid Mech 1982;118:341–77.
[19] Givi P. Model-free simulations of turbulent reactive flows. Prog energy Combust Sci 1989;15(1):1–107.
[20] Lesieur M, Metais O. New trends in large-eddy simulations of turbulence. Annu Rev Fluid Mech 1996;28(1):45–82.
[21] Ferziger JH, Perić M. Computational methods for fluid dynamics, vol. 2. Springer Berlin; 1999.
[22] Boussinesq J. Théorie de l'écoulement tourbillant (theories of swirling flow), mém. prés. par div. savants à l'acad. Sci Paris 1877;23.
[23] Menon S, Yeung PK, Kim WW. Effect of subgrid models on the computed interscale energy transfer in isotropic turbulence. Comput fluids 1996;25(2):165–80.
[24] Yoshizawa A, Horiuti K. A statistically-derived subgrid-scale kinetic energy model for the large-eddy simulation of turbulent flows. J Phys Soc Jpn 1985;54(8):2834–9.
[25] Nakayama A, Vengadesan SN. On the influence of numerical schemes and subgrid–stress models on large eddy simulation of turbulent flow past a square cylinder. Int J Numer methods fluids 2002;38(3):227–53.
[26] Moeng Chin-Hoh, Wyngaard John C. Spectral analysis of large-eddy simulations of the convective boundary layer. J Atmos Sci 1988;45:3573–87.
[27] Yang C, Lohner R, Lu H. An unstructured-grid based volume-of-fluid method for extreme wave and freely-floating structure interactions. J Hydrodynamics, Ser. B 2006;18(3):415–22.
[28] Yang C, Lohner R, Yim SC. Development of a CFD simulation method for extreme wave and structure interactions. In: Proceeding of 24th Int. conference on offshore Mech. And Arctic Eng. (OMAE2005), Halkidiki, Greece; 2005. p. 12–7.
[29] Chen G, Kharif C, Zaleski S, Li J. Two-dimensional navier–stokes simulation of breaking waves. Phys fluids 1999;11:121.
[30] He X, Chen S, Zhang R. A lattice boltzmann scheme for incompressible multiphase flow and its application in simulation of rayleigh-taylor instability. J Comput Phys 1999;152(2):642–63.
[31] Hirt CW, Nichols BD. Volume of fluid (VOF) method for the dynamics of free boundaries. J Comput Phys 1981;39(1):201–25.

[32] Gebreslassie Mulualem G, Tabor Gavin R, Belmont Michael R. Cfd simulations for sensitivity analysis of different parameters to the wake characteristics of tidal turbine. Open J Fluid Dyn 2012;2:56.
[33] Gebreslassie Mulualem G, Tabor Gavin R, Belmont Michael R. Numerical simulation of a new type of cross flow tidal turbine using openfoam–part ii: investigation of turbine-to-turbine interaction. Renew Energy 2013;50:1005–13.
[34] Gebreslassie Mulualem G, Tabor Gavin R, Belmont Michael R. Cfd simulations for investigating the wake states of a new class of tidal turbine. J Renew Energy Power Qual 2012;10(241).
[35] MacLeod AJ, Barnes S, Rados KG, Bryden IG. Wake effects in tidal current turbine farms. In: International conference on marine renewable energy-conference proceedings; 2002. p. 49–53.
[36] Nishino T, Willden RHJ. Effects of 3-d channel blockage and turbulent wake mixing on the limit of power extraction by tidal turbines. Int J Heat Fluid Flow October 2012;37:123–35.
[37] Mikkelsen R. Actuator disc methods applied to wind turbines [PhD thesis]. Technical University of Denmark; 2003.
[38] Sanderse B. Aerodynamics of wind turbine wakes. Petten, The Netherlands: Energy Research Center of the Netherlands (ECN), ECN-E–09-016; 2009. Tech. Rep.
[39] Houlsby GT, Draper S, Oldfield MLG. Application of linear momentum actuator disc theory to open channel flow. 2008. Technical report, Technical Report 2296–08, OUEL.
[40] Garrett C, Cummins P. The efficiency of a turbine in a tidal channel. J Fluid Mech 2007;588:243–51.
[41] Whelan JI, Graham JMR, Peiro J. A free-surface and blockage correction for tidal turbines. J Fluid Mech 2009;624:281–91.
[42] Myers L, Bahaj AS. Wake studies of a 1/30th scale horizontal axis marine current turbine. Ocean Eng 2007;34(5–6):758–62.
[43] Weller HG, Tabor G, Jasak H, Fureby C. A tensorial approach to computational continuum mechanics using object orientated techniques. Comput Phys 1998;12(6):620–31.